Spatial Filtering for Enhanced High-Density Surface Electromyographic Examination of Neuromuscular Changes and Its Application to Spinal Cord Injury

Xu Zhang (xuzhang90@ustc.edu.cn)
University of Science and Technology of China https://orcid.org/0000-0002-1533-4340
Xinhui Li
University of Science and Technology of China
Xiao Tang
University of Science and Technology of China
Xun Chen
University of Science and Technology of China
Xiang Chen
University of Science and Technology of China
Ping Zhou
University of Texas Health Science Center at Houston

Research

Keywords: electromyography, noninvasive diagnosis, neuromuscular changes, spatial filtering, spinal cord injury

Posted Date: March 17th, 2020

DOI: https://doi.org/10.21203/rs.3.rs-17567/v1

Version of Record: A version of this preprint was published on December 3rd, 2020. See the published version at https://doi.org/10.1186/s12984-020-00786-z.

Spatial Filtering for Enhanced High-Density Surface Electromyographic Examination of Neuromuscular Changes and Its Application to Spinal Cord Injury

[1]Xu Zhang, [1]Xinhui Li, [1]Xiao Tang, [1]Xun Chen, [1]Xiang Chen, and [2]Ping Zhou

[1]School of Information Science and Technology, University of Science and Technology of China, Hefei, Anhui 230027, China.

[2]Department of Physical Medicine and Rehabilitation, University of Texas Health Science Center at Houston, and TIRR Memorial Hermann Research Center, Houston, TX, USA.

Address Correspondence to:

Xu Zhang, PhD

Neuromuscular Control Laboratory

Biomedical Engineering Program

University of Science and Technology of China(USTC)

443 Huangshan Rd, USTC West Campus, Electronic BLDG 3, Suite 814

Hefei, Anhui Province 230027 China

Tel: +86-551-63601175

Email: xuzhang90@ustc.edu.cn

Abstract

Background: Spatial filtering of multi-channel signals is considered to be an effective pre-processing approach for improving signal-to-noise ratio. The use of spatial filtering for preprocessing high-density (HD) surface electromyogram (sEMG) helps to extract critical spatial information, but its application to non-invasive examination of neuromuscular changes have not been well investigated.

Methods: Aimed at evaluating how spatial filtering can facilitate examination of muscle paralysis, three different spatial filtering methods are presented using principle component analysis (PCA) algorithm, non-negative matrix factorization (NMF) algorithm, and both combination, respectively. Their performance was evaluated in terms of diagnostic power, through HD-sEMG clustering index (CI) analysis of neuromuscular changes in paralyzed muscles following spinal cord injury (SCI).

Results: The experimental results showed that: 1) The CI analysis of conventional single-channel sEMG can reveal complex neuromuscular changes in paralyzed muscles following SCI, and its diagnostic power has been confirmed to be characterized by the variance of Z-scores; 2) the diagnostic power was highly dependent on the location of sEMG recording channel. Directly averaging the CI diagnostic indicators over channels just reached a medium level of the diagnostic power; 3) the use of either PCA-based or NMF-based filtering method yielded a

greater diagnostic power, and their combination could even enhance the diagnostic power significantly.

Conclusions: This study not only presents an essential preprocessing approach for improving diagnostic power of HD-sEMG, but also helps to develop a standard sEMG preprocessing pipeline, thus promoting its widespread application.

Keywords: electromyography, noninvasive diagnosis, neuromuscular changes, spatial filtering, spinal cord injury

1. Introduction

Spinal cord injury (SCI) is a leading cause of adult disability worldwide [1]. The disruption of communication between the brain and the spinal cord results in both loss of voluntary movement (paraplegia) and loss of sensation [1], [2]. However, the effect of a paraplegia on the survival and function of motor unit (MU) in pathological muscles remains unclear. Since the MU is regarded as the basic functional unit and the final pathway of the neuromuscular control system, it is of great importance to identify MU changes induced by specific mechanisms following the SCI [3], which can offer guidance for the design of effective SCI rehabilitation protocols.

In clinical routine, an invasive approach using concentric needle is applied to electrophysiological examination of MU properties [4], [5]. The insertion of the needle, however, has to deal with various issues including the invasive discomfort, a requirement of medical supervision and a risk of infection, limiting its wide applications including long-term monitoring and repetitive investigations [6]. In addition, the subjectivity during diagnostic evaluation based on the experience of the professional clinicians remains the most important factor when it comes to examine neuromuscular changes [7]. As a result, there is a huge demand for an objective, quantitative and noninvasive approach for convenient examination of neuromuscular diseases and injuries.

Surface EMG (sEMG) recording using electrodes placed over skin surface provides an alternative tool for examining neuromuscular behaviors in a noninvasive manner. The centimeter-size probe of the conventional surface electrode, however, may not be as selective as the invasive needle. A low-pass filtering effect of the conduction volume including skin fat tissues also impacts the sharpness and amplitude of the MU waveforms, thus attenuating much useful information. Therefore, the recorded sEMG signal generally presents an interference pattern where any single MU waveform cannot be visually discerned [8]. As a result, conventional sEMG has not been well accepted by clinicians. Recently, many attempts have been made in the academic society toward clinical applications of sEMG, especially for examination of neuromuscular changes [9]. Many important indicators have been extracted from the time domain, the frequency domain and the time-frequency domain of the sEMG signals [10]. For example, Jensen *et al.* [15] applied sEMG amplitude, mean and median frequency to quantify pericrancial muscles in headache. Kaplanis *et al.* [14] introduced a multiscale entropy-based approach for automated sEMG classification of neuromuscular disorders. Clustering index (CI) was proposed by Uesugi *et al.* [16] to quantitatively evaluate the clustering degree of sEMG. It enables effective discrimination between neurogenic and myopathic changes using the morphology of the surface EMG signals [17], [18]. The CI analysis has achieved great success in non-invasive diagnosis of diseases such as stroke and amyotrophic lateral sclerosis [19].

In recent years, high-density sEMG (HD-sEMG) techniques have been widely used with a flexible grid of closely arranged electrodes coving the active muscle zone. The large area of the grid enables the full and comprehensive characterization of the neuromuscular activity [22]. This technique can be used to collect important spatial information concerning muscle activation, thus being able to reflect the heterogeneity of the muscle activation. Successful applications including the location of muscle tendon units [23] and innervation zones [24], and the estimation of muscle fiber conduction velocities [25] have been reported. The revealed muscle heterogeneity also contributes to an accurate depiction of muscle activity. It has been proven to facilitate the high-precision estimation of muscle force [26]. In addition, using spatial information of HD-sEMG has benefit to eliminate cross-talk of channels. Since single-channel sEMG measurements are from the activities of different co-contracting muscles or the superposition of different MUAP waveforms of the same muscle, HD-sEMG helps to distinguish these different sources and extract the activity characteristics of individual muscles and even individual MUs [27]. All these prominent features of applying the HD-sEMG techniques can be further promoted by the use of spatial filtering.

Spatial filtering is aimed to reduce redundancy of HD-sEMG and highlight useful information based on activation heterogeneity, thus improving the SNR of the signals. Many matrix factorization algorithms have been successfully developed for the design of spatial filters in processing sEMG data with various goals. For example, Staudenmann *et al.* [28] conducted PCA-based spatial filtering method on

129 the sEMG signals to improve the quality of force prediction. Harrach *et al.* [29] used
130 canonical correlation analysis to extract the activity of a targeted muscle from the
131 possible interference of con-contracting muscles. Chen *et al.* [30] used independent
132 component analysis to locate muscle-tendon units during dynamic motion tasks.
133 Gazzoni *et al.* [31] applied NMF to quantify sEMG activity spatial distribution on
134 the forearm for sake of the optimization of electrode configuration for sEMG-based
135 control of prostheses. Although these algorithms have been widely used in the
136 research fields of biomechanics, neuro-prosthetic control and sport analyses [32], the
137 spatial filtering of sEMG data has not well investigated toward diagnosis of
138 neuromuscular changes.

139 It is hypothesized that spatial filtering can help to enhance and mine useful
140 diagnostic-related information of HD-sEMG, thus improving diagnostic power of
141 sEMG. In order to verify this hypothesis, two common algorithms, namely the PCA
142 and the NMF algorithms, were selected for performing the spatial filtering. The PCA
143 algorithm is able to identify the major sources of variation and detect this type of
144 redundancy and noise in multivariate data [35]. Therefore, the PCA-based spatial
145 filtering method is widely used to remove redundant common information, noise
146 artifacts, and possible cross-talks of HD-sEMG **Error! Reference source not found.**, [37].
147 The NMF algorithm is able to extract specific components of the input multi-channel
148 sEMG signals, and these components are physiologically understood as the basic
149 spatial patterns termed muscle synergies driven by the central nervous system to
150 formulate muscle activities. It can be used as an effective tool for localizing different

activation sub-regions of a muscle during voluntary contractions. Therefore, three spatial filtering methods were selected as representative solutions for pre-processing the HD-sEMG data in this study: the PCA-based method, the NMF-based method and the method with a combination of both PCA and NMF algorithms. Our work not only applies the sEMG CI examination to the SCI data to investigate neuromuscular changes, but also proves the benefit of applying spatial filtering to HD-sEMG data for improving CI diagnostic power. Meanwhile, it evolves the PCA-NMF-based spatial filtering method, which helps to form a standard pipeline for HD-sEMG preprocessing before its clinical applications including diagnosis of neuromuscular changes.

2. Methods

2.1 Subjects

Nine subjects with incomplete cervical SCI (S1-S9, ASIA C or D) were recruited from the Clinical Neuroscience Research Registry at the Chicago Rehabilitation Institute (Chicago, IL). Demographic and clinical measures for the subjects with SCI are summarized in Table 1. In addition, thirteen neurologically intact subjects and (C1-C13) without any neuromuscular disorder or injury also participate into the experiments.

2.2 Experiments

The abductor pollicis brevis (APB) muscle was examined in this study. The data collection experiments were conducted on both sides of the subjects with SCI respectively, in a random order. The same experimental procedure was just applied to a randomly selected side of each control subject. On this basis, all the tested muscles can be categorized into three groups: the muscles on the left side of subjects with SCI (denoted as SCI-left group), the muscles on the right side of subjects with SCI (denoted as SCI-right group) and the control muscles from the neurologically intact subjects (denoted as control group). A flexible electrode array consisting of 64 electrodes in an 8×8 grid formation was used to target at the examined APB muscles, as shown in Fig. 1. Each electrode had a round recording probe in a diameter of 1.2 mm, and the center-by-center distance was 4 mm between two consecutive electrodes. The surface EMG signals were collected by a Refa128 EMG Recording

System (TMS International BV, Enschede, The Netherlands) in 64 recording channels as a result of mono-polar configuration. The sampling rate was set at 2 kHz per channel. There is another round electrode (Dermatrode; American Imex, Irvine, CA) placed over olecranon of the tested arm as the ground reference for the recording system.

The experiment was carried out in a quiet room in order to reduce the impact of the environmental noises. During the experiment, subjects were seated in a comfortable mobile chair. Their tested arm was bent approximately 90 degrees and was placed on a height-adjustable desk. In the beginning of the experiment, the subject was encouraged to perform three maximal voluntary contractions (MVCs). The maximum value of these trials determined by monitoring the EMG amplitude was taken as a valid MVC. Then the subject was asked to generate an isometric contraction by performing elbow flexion with increasingly graded force levels, roughly corresponding to 10%, 30%, 50%, 70%, submaximal (90%) and maximal voluntary contraction (MVC) in terms of the MVC percentage via the EMG amplitude. The subject was encouraged to remain at least 3 second as stable as possible for each contraction level. Sufficient rest was also allowed to avoid muscle fatigue between two consecutive trials.

The raw HD-sEMG data collected from all muscles were imported to the MATLAB (Version R2016a, MathWorks, Natick, MA, USA) software for analysis. Fig. 2 shows the entire framework for examining neuromuscular changes through

spatial filtering analysis and subsequent CI analysis of the HD-sEMG data, with more details described as follows.

2.3 Signal preprocessing

A fourth-order Butterworth band-pass filter at 20-500Hz was applied to eliminate potential low-frequency noises (e.g., motion artifacts) and high-frequency interferences. Then, a set of second-order notch filters were used to remove the 50-Hz power line interference and its harmonics. Subsequently, the spatial filtering methods could be applied to the HD-sEMG data.

1) Spatial Filtering using PCA

The PCA algorithm can transform multi-dimensional data into a set of linearly uncorrelated elements called principal components (PCs) onto which the original data are projected. The calculation of PCs is realized by diagonalization of the covariance matrix of data. Suppose the original signal $\mathrm{M}^{\mathrm{m\times t}}$ is m row and t columns, m represents the number of channels (64 in this study), t is the sEMG signal sampling points. The covariance of $\mathrm{M}^{\mathrm{m\times t}}$ was calculated as Eq. (1).

$$\mathrm{cov(M)} = (\sum_1^t(\mathrm{M}_i - \mu_1) * (M_j - \mu_2))/(n-1). \quad (1)$$

where M_i and M_j represent the *i*-th and *j*-th row of the $\mathrm{M}^{\mathrm{m\times t}}$, and μ_1 and μ_2 represent their mean values. Then the eigenvalue λ and the eigenvector X were calculated to decompose 64-channel sEMG signals into 64 PCs $[\mathrm{X}_1, \mathrm{X}_2, \dots, \mathrm{X}_{64}]$ corresponding to their eigenvalues ($\lambda_1 \geq \lambda_2 \geq \cdots \geq \lambda_m > 0$) in a descending order. The eigenvectors describe the spatial distribution of the projected EMG over the grid

that evolves in time. It has been supposed that the high eigenvalues of the first two components carry a substantial amount of redundant information (i.e., common mode) among multiple channels, and the components corresponding to the smallest few eigenvalues contain measurement noises unrelated to EMG signals [28], **Error! Reference source not found.**, [38]. Therefore, it is necessary to remove these components. In this study, the PCs with the largest two eigenvalues and four smallest eigenvalues were intentionally selected and discarded, and therefore the remaining PCs $[\mathrm{X}_3, \mathrm{X}_4, \ldots, \mathrm{X}_{60}]$ were used to reconstruct the filtered signal $M'^{\mathrm{m}\times\mathrm{t}}$.

2) Spatial Filtering using NMF

The NMF algorithm has been proven to be successful in processing multichannel sEMG signals and its outcomes have very strong physiological interpretations in muscle synergy analysis. This algorithm is formulated as a solution to a minimization problem with nonnegative bound constraints [40]. In this study, the multi-channel normalized sEMG profile matrix $\mathrm{M} \in R^{m\times t}$ (m channels, t samples) was decomposed into two non-negative matrices $\mathrm{W} \in R^{m\times s}$ and $\mathrm{C} \in R^{s\times t}$ (where s<m) by the NMF algorithm according to Eq. (2).

$$\mathrm{M}^{\mathrm{m}\times\mathrm{t}} = \mathrm{W}^{\mathrm{m}\times\mathrm{s}}\mathrm{C}^{\mathrm{s}\times\mathrm{t}}. \tag{2}$$

The matrix W can be interpreted as a number s of muscle synergies, while the matrix C represents their corresponding time-varying activation coefficients. For processing the HD-sEMG data recorded on an entire muscle, each column of W here represents a spatially correlated activation pattern over the m-channel electrode array. Given the structural and functional heterogeneity of muscle activation, such an

activation pattern may reflect the localization of a specific signal source. Its internal physiological explanation may be a muscle tendon unit or the muscle belly. Thus, each row of the matrix C here specifies how an activation pattern is modulated during the task performance. The variable *s* varies from 1 to *m*, representing the number of activation patterns and it can be decided by repeating the NMF analysis. In this study, *s* was set to 2 according to previous recommendation that two activation patterns were sufficient to account for most of the sEMG activities [37]. Matrix decomposition algorithm was used to minimize the cost function defined as square of the Euclidean distance. The corresponding multiplicative iteration rule not only ensures the non-negative property of the matrixes, but also allows the algorithm to converge to the local optimal solution.

The area covered by a time-varying coefficient vector was calculated to define the activation intensity of the corresponding activation pattern.

$$Intensity(i) = \sum_{j=1}^{t} C_i(j), \quad (3)$$

Where C_i represents the ith time-varying coefficient vector and *t* is the length of the sample. The activation pattern corresponding to the highest *Intensity* values was considered to be the major activation pattern. The channels whose weighting factors ranked the first quarter in the major activation pattern contributed the motor pattern. Thus, the first 16 channels that had larger weighting factors were sorted out from the major activation pattern in this work, and these corresponding channel sEMG of original input was selected as the output.

2.4 Data segmentation and CI analysis

The data (in a form of multiple channels regardless of whether they were spatially filtered or not) presented several segments of sEMG activities according to the experiment protocol. The onset and offset of each sEMG activity burst can be easily determined. For CI analysis, a series of 1-s epochs (equivalent to 2000 sample points at the sampling rate of 2000 Hz) need to be segmented from the EMG activity. The epochs were deliberately chosen from stable isometric muscle contractions at a certain force level and those epochs with obvious muscle force variation were discarded. Thus, the number of epochs in a multi-channel form ranged from 20 to 40 over all force levels for each of all subjects.

CI is a non-invasive quantitative method for analyzing uneven distribution and cluster of the processed signal to different neurogenic and myopathic changes [17]. To calculate CI, the signal in each epoch was divided into several non-overlapping consecutive windows in length of 15 ms, which is regarded to approximately cover an individual MUAP [16]. Suppose that there are K windows in total derived in an epoch and Ai was the area of each window. The differential sequences between every consecutive area value (DA_i), between every second window (DB_i) and between every third window (DC_i) can be calculated.

Then the CI of each epoch is defined as:

$$\mathrm{CI} = \{\sum_{i=1}^{K-1} DA_i^2 + \sum_{i=1}^{K-2} DB_i^2 + \sum_{i=1}^{K-3} DC_i^2\}/(6 \cdot \sum_{i=1}^{K} A_i). \quad (4)$$

The CI has a value between 0 and 1, and a relatively high value represents a highly clustered signal, appearing with isolated large action potentials. If the EMG

292 epoch carries multiple channels (it is always the case in this study), the average CI
293 value was calculated from all chosen channels. While the values of CI depended on
294 the contraction level: the increase in contraction levels resulted in a lower value, the
295 area of each epoch, that is the area of all windows, was used to estimate the muscle
296 contraction level [16]. It had been proven to be linearly related to CI values using
297 double logarithmic scale [18]. Hereafter, the average areas for all selected channels
298 on each epoch were calculated. For each analysis epoch on the same muscle, two
299 values were obtained: a mean log (area) and a mean log (CI), which were expressed
300 as a point in the CI-area plot. The points derived from the analysis epochs can be
301 scattered to form a cloud over the CI-area plane.

302 The quantification of the normal data reference in the CI-area plot is the
303 prerequisite to subsequent diagnosis. To establish the distribution of the normal
304 cloud, a linear regression analysis was performed on all analysis epochs ($1 \leq \text{area} \leq$
305 $100\mu V \cdot \text{sec}$)from the healthy subjects was performed for both log(CI) and log(area).
306 For each epoch, the deviation of the log (CI) scale from the linear regression line was
307 calculated. Then these deviation values were averaged to obtain a mean residual
308 (denoted as Rm), which can be used to assess the presence of abnormality for each
309 subject. The mean u and standard deviation (σ) of the Rm values on the two sides
310 of all the subjects were calculated and then a Z-score was computed as the final
311 quantify indicator for the evaluation,

312 $$Z = (Rm - \mu)/\sigma. \quad (5)$$

A Z-score between ± 2.5 was defined as abnormal. A tested muscle with a Z-score higher than +2.5 indicated neurogenic changes while a Z-score lower than -2.5 was diagnosed as being myopathic changes.

2.5 Performance evaluation and statistical analysis

To evaluate the effect of spatial filtering in HD-sEMG-based diagnosis, the PCA-based method, the NMF-based method and their combination termed the PCA-NMF-based method were applied for spatial filtering of the HD-sEMG signals, with comparison of the original HD-sEMG without any spatial filtering approach. In the PCA-NMF-based method, both the PCA method and the NMF method were implemented sequentially. Regardless of whether the data were spatially filtered or not, the diagnostic analyses relied on application of the CI method to HD-sEMG data recorded from three muscle groups: SCI-left group, SCI-right group and control group.

Given a certain group of examined muscles, both the abnormal CI Z-core increase and decrease can be simultaneously observed due to diversity of abnormality following SCI. This was the case in this study (as reported in the following Results Section). For a specific muscle with certain abnormal changes, the greater Z-score dispersion from the normal range was yielded by the examination approach (including the signal pre-processing method), the higher its diagnostic sensitivity became according to the CI calculation. On this basis, the variance of Z-scores over a group of tested muscles could be used to evaluate the diagnostic sensitivity of the CI

indicators after different spatial filtering methods. Suppose the Z-score variance was a_{SCI} and $a_{control}$ calculated over a group of tested muscles from subjects with SCI and healthy controls, respectively. The value of $a_{control}$ of each tested muscle is 1 due to the defined normalization of diagnostic criteria in the CI method. The evaluation criterion abnormality discriminating index (ADI) was defined as a quantitative indicator of evaluating diagnostic power of the entire examination approach according to Eq. (6), which represents the sensitivity of identifying various types of neuromuscular changes from abnormal signals.

$$ADI = \frac{a_{SCI}}{a_{control}}. \quad (6)$$

The ADI values were calculated respectively under different conditions. In this study, the condition was defined by the use of both the channel and the spatial filtering method for data analysis. A special condition was designed as a representative approach without any spatial filtering method for the comparison purpose, which simply averaged CI values over all used channels when HD-sEMG data were used. The higher an ADI value was yielded, the greater diagnostic sensitivity (to various alternations in the given subject population) the corresponding method had.

In order to verify the generally sequential consistency of individual muscles' diagnostic outcomes, a series of linear regression analyses were performed on the CI Z-scores derived from all muscles (in both the SCI-left and SCI-right groups), between any two different conditions. Two separate two-way repeated-measure ANOVAs were performed on the Z-score, with the group (two levels: the control

muscle group versus each of two muscle group with SCI, respectively) considered as the between-subject factor and the condition (four levels: the simply averaging approach and three spatial filtering methods) considered as the within-subject factor, to simultaneously examine their effect on the Z-score group means. Another two-way repeated-measure ANOVA was performed, with both the side/group (two levels: the SCI-left group versus the SCI right group) and the condition (four levels) considered as within-subject factors. The level of statistical significance was set to $p < 0.05$ for all above analyses. All statistical analyses were completed using SPSS software (ver. 22.0, SPSS Inc. Chicago, IL).

3. Results

Fig. 3 shows the resultant CI-area plot of the scattered data points from three muscle groups in the double logarithmic scale, when the data were only from a deliberately selected channel. For the normal cloud consisting of all data points from the control muscle group, the CI showed a decreasing trend as the contraction level increased. This was suitable for a linear regression analysis ($y = -0.0631x - 0.5470$). Along the regression line, there is a banding region that can well characterize the distribution region of the normal cloud.

Fig. 4 reports the CI Z-scores when using data from each of four different channels (channel 28, channel 31, channel 37 and channel 64). It can be seen that although different CI Z-scores and the corresponding diagnostic results obtained from different channels, the order of the CI Z-scores was substantially the same. For example, for the left muscle of S8, data from channel 31 gave a diagnosis of abnormal increase, but the other three channels failed to report any abnormality. Using data from channel 37, the left muscle of S8 had a CI value that approximated to the upper limit of the normal boundary. It is surprisingly to find that the CI Z-score value of S8 was always the highest on the SCI-left group. Similar observations can also be found in multiple cases such as S2, S7 and S9 on the SCI-left group and S1 on the SCI-right group. Further, for different channels, the data of the same group exhibited different degrees of dispersion. More abnormal diagnostic conclusions could be found for the group with high dispersion. It was confirmed that the ADI value was able to be used to judge the diagnostic power.

Therefore, using four different channels had an impact on the diagnostic power, quantified by the ADI ranging from 2.3160 to 14.0252 for the SCI-left muscle group and 2.5341 to 5.7445 for the SCI-right group.

Fig. 5 reports the resultant Z-scores derived from multi-channel data for all the examined muscles when different spatial filtering methods were used respectively. The CI Z-scores from the same group of muscles almost had a consistent order even comparing to that at any single channel in Fig. 4, regardless of whether the data were filtered by any spatial filtering method or not. When different spatial filtering methods were applied, however, the muscle with an abnormal decision had varied dispersions from the normal boundary. Specifically, the Z-scores obtained by simply averaging CI values over all used channels were shown in Fig. 5a. Although some muscles were reported to be abnormal, their Z-scores were extremely close to the normal boundary, and the ADI value was reported to be 2.4936 for the SCI-left group and 2.1671 for the SCI-right group. Both ADI values were found to remain at a median level of the values derived from individual channels. After spatially filtering the HD-sEMG data using three methods, more abnormal Z-scores are exhibited in Fig. 5b-d, and their dispersions from the normal boundary are relatively expanded as well. Thus, it is not accidentally that the ADI values were improved to 3.1488 for the SCI-left muscle group and 3.8785 for the SCI-right muscle group using the PCA-based method. Both values were 8.0397 and 3.8033 using the NMF-based method. Apparently, the PCA-NMF-based method presented the highest degree of Z-score dispersion, and meanwhile it was able to reveal more abnormal

muscles. For example, the use of the PCA-NMF-based method successfully produced abnormally high Z-scores for the S3 and S5 on the SCI-right group, whereas the use of any other spatial filtering method or any single channel failed to reveal any abnormality. Finally, the ADI values yielded by the PCA-NMF-based method reached to 13.9157 for the SCI-left group and 11.7014 for the SCI-right group, which approximated into or even exceeded the maximal level of the ADI values derived from individual channels.

The linear regression analyses reported strong correlations (R2 from 0.80 to 0.93) between the CI Z-scores made by any spatial filtering method and the simply averaging approach (i.e., no spatial filtering method), and estimates of coefficients were all statistically significant ($p < 0.001$). The ANOVAs revealed no significant main effect of the group and no significant difference in group means of the CI Z-score between any muscle group following SCI and the control muscle group, or no significant main effect of the spatial filtering method ($p = 0.855$) on the CI Z-score. However, significant difference was found between the SCI-left muscle group and the SCI-right muscle groups ($P<0.05$).

The final ADI values derived from original sEMG data at four individual channels and spatially filtered HD-sEMG data via different spatial filtering methods were summarized in Table 2. It showed that the ADI values of different channels might be quite different. Comparing to the simply averaging HD-sEMG data without any spatial filtering, the PCA and NMF spatial filtering methods had larger ADI values on both the SCI-left and the SCI-right groups. Moreover, the PCA-NMF-based

433 spatial filtering method outperformed other methods by yielding almost the largest

434 ADI values on both groups of muscles following SCI.

435

436 # 4. Discussion

437 This study introduced three spatial filtering methods for preprocessing HD-sEMG
438 data to enhance the power of assessing neuromuscular abnormalities following SCI.
439 The primary findings of the current study include:1) the complex neuromuscular
440 changes following SCI were revealed by the CI analysis of conventional
441 single-channel sEMG, and the diagnostic power could be characterized by the
442 variance of Z-scores derived from a group of subjects; 2) The diagnostic power was
443 found to vary across positions of individual channels for recording sEMG data, and it
444 only remained at a median level when all the CI values derived from all recording
445 channels were simply averaged; 3) The application of PCA-based filtering method or
446 NMF-based filtering method helped to improve the diagnostic power significantly,
447 and the method with their combination outperformed any single method in terms of
448 diagnostic power; 4) A subject with SCI might have pathological changes on both
449 sides of muscles in different types and at different degrees.

450

451 ## 4.1 MU alternations following SCI evaluated by CI method

452 The CI method was traditionally used for single-channel sEMG analysis.
453 Regardless of any channel (within the array) used for analysis, it can be observed
454 from Fig. 4 that each examined muscles tended to have a consistent decision.
455 Furthermore, all muscles from subjects with SCI exhibited three different CI patterns
456 including normal and abnormal increase and decrease of the CI indicator.

Four muscles of the SCI subjects had an abnormal CI Z-score increase indicating neurogenic changes. These changes can be attributed to loss of MUs and subsequent reinnervation of denervated muscle fibers. The MU loss may take place after gray matter is destroyed at and near the lesion epicenter and it can lead to a decrease in the number of activable MUs and denervation of muscle fibers [3]. Complete denervation due to motoneuron degeneration eliminates voluntary control of the affected muscle fibers. Subsequently, the surviving MUs tend to undergo adaptive changes, such as muscle fiber reinnervation for a functional supplement, thus contributing to an abnormal enlargement of their structures [41]. These enlarged MUs lead to abnormal MUAPs with large amplitude and multiple phases, overlying into scattered and isolated EMG signals. In addition, after chronic (>1 year) SCI, MU properties of human hand muscles shifted towards decreased firing rate and increased firing synchronization [42]. Simultaneously, other altered MU control properties including the compression of MU recruitment threshold and the supplementary recruitment of enlarged MUs during muscle contraction might also lead to an abnormal increase of CI [2], [43].

Eleven muscles had abnormally lower Z-scores indicating myopathic changes, which could be related to muscle fiber disuse atrophy. Atrophied and angular muscle fibers could lead to partial denervation, which can be indicated by intramuscular motor axon sprouting, an important compensatory mechanism for recovery of muscle innervation after death of some motoneurons [44]. A selective degeneration of the

relatively larger and superficial MUs may be another reason. Thus the induced flatter and denser surface EMG signals would make decreased CI values.

The resultant Z-scores of remaining muscles were located within the normal range. However, substantial muscle weakness was also found in these muscles. Their paralyses are likely to be attributed to a deficit of descending central drive as a result of the severance of central nervous system axons and demyelination of central or peripheral axons, while the affected muscles still function more or less normally [45]. Although the number of activable MUs drops, their recruitment and control property remains similar to those of healthy controls. Thus, these muscles could only deliver a fraction of the normal voluntary drive, leading to corresponding muscle weakness [45]. Another possible explanation for the distribution in the "normal range" might be a combined or cancelled effect of both neurogenic and myopathic processes [46]. Moreover, the effect of injury on the lesion spinal cord segment and denervation of muscle fibers might be contributors to muscular weakness [42]. Therefore, the experimentally observed CI variations in paralytic muscles can be viewed as the overall or collective effects of these different factors [18].

As a result, the experimentally observed CI abnormality consists of two patterns, which lead to CI deviation in two different directions, respectively. Therefore, a pooled analysis of a group of paralyzed muscles following SCI can allow their CI indicators to spread from the centered normal range, indicating that there are complex neuromuscular changes following SCI. This phenomena explains why there was no significant difference in group means of CI Z-scores in the ANOVAs, and

500 therefore the ADI was more appropriate to characterize the diagnostic power of the
501 CI method in this study.
502
503 **4.2 Examination with HD-sEMG recording**
504 Given the HD-sEMG recording, varied distributions of the CI Z-scores were
505 observed and thus different diagnostic decisions were made when data from different
506 channels were used (see Fig.4). Thus, it also directly led to different diagnostic
507 power quantified by the ADI value. This confirms our previous assumption that the
508 important diagnostic information is likely to be derived from some local regions of
509 the electrode array due to the heterogeneity of the targeted muscle. This finding also
510 suggest a risk of electrode placement when applying the routine single-channel
511 sEMG recording, while its clinical application has been increasingly investigated
512 toward noninvasive examination. Depending on the placement of the sEMG
513 electrode (targeting at a local region of the examined muscle), the CI diagnostic
514 decision varied a lot, probably leading to controversial results. This may
515 dramatically impact the usability of the sEMG examination. In addition, we also
516 found that the channel with the highest diagnostic power was not always located at
517 the center of the array or over the position of main muscle belly. Such a finding
518 further indicates the importance of electrode placement since the channel location
519 yielding the most diagnostic power is usually uncertain solely relying on anatomical
520 knowledge.

Taking the averaged CI value over HD-sEMG channels is the most straightforward method to extract the global information of muscle activity and eliminate the influence of the electrode position. However, unsurprisingly, we found that the ADI diagnostic power obtained in this way was only at the median level of those using individual channels. This shows that simply averaging may smooth or cancel the useful diagnostic information present in the local channels, which is detrimental to revealing specific abnormalities in individual muscles. In this case, the resultant CI indicator reflected poor understanding of underlying pathological muscle changes.

4.3 The Advantages of Spatial Filtering

The improved performance yielded by the use of either PCA-based or NMF-based spatial filtering method in terms of increased ADI value can demonstrate the efficiency of applying the spatial Filters. Furthermore, the strong correlations revealed by the regression analyses between individual muscles' Z-scores derived from any spatial filtering method and the simply averaging approach indicate consistency of their diagnostic decisions (they are able to produce or tend to produce the same type of abnormality for specific muscles). These findings suggest that the use of spatial filters enhances the sensitivity of HD-sEMG CI indicator to various neuromuscular changes.

The PCA-based filtering method was designed to deliberately remove PCs representing homogeneously changing and common features, and detail PCs

representing high-frequency noise and cross-talk [28], [36]. Such processing helps to enhance regional difference of the signal and is considered to be the main reason for diagnostic power improvement by the PCA-based spatial filtering method. Unlike the PCA algorithm, the NMF algorithm extracts physiologically relevant components from the signal, called muscle synergy, which describes the regions of muscle contraction synchronization [43], [45]. In this way, the NMF-based method is equivalent to a channel-selection method by extracting these muscle synergy components. The method is actually a dimensionality reduction processing that locates and highlights the main areas within the HD-sEMG array contributing into muscle activities.

According to their calculation principles, both algorithms were regarded to emphasize different aspects of information convoyed in the raw HD-sEMG data. As a result of their complementary effect, it is easy to explain that their combination can further improve the diagnostic power in comparison to sole use of the PCA-based or the NMF-based method.

The HD electrode array physically covers the examined muscles, providing a wealth of spatial information in a large area. Direct averaging these channels is not satisfactory for diagnostic improvement. By contrast, spatial filtering methods evidently improve the performance of HD-sEMG examination, approximating to the maximal level of diagnostic powers when individual channels are used. Thus, the use of spatial filtering helps to highlight and refine useful diagnostic information associated with heterogeneity of the muscle activation, and provides a necessary and

convenient approach to pre-process HD-sEMG data for further examination of neuromuscular changes. In addition to enhancing diagnostic power, this can also minimize the potential influence of electrode placement. The spatial filtering of HD-sEMG can facilitate sEMG examination, indicating the ease of reflecting potential abnormality in certain muscles by the means of a noninvasive approach.

4.4 Difference between two sides of the subject with SCI

Since the CI analysis performed the examination of individual muscles, it is straightforward to compare the neuromuscular changes in muscles on both side muscles of a subject. It was observed that the two side muscles of some SCI subjects showed different CI decisions. For example, the left muscles of S1, S3 and S5 were diagnosed as being ‘myopathy’ while their contralateral muscles were diagnosed as being ‘neurogenic’ changes. This may be attributed to the asynchrony of the left and right muscles. When the physiological balance is broken following SCI, it always overcorrects so that the left and right muscles may present different types of neuromuscular changes at different degrees.

4.5 Limitations of the current work and future expectations

This paper just focuses on the application of spatial filtering and presents only three types of common spatial filtering methods. Another issue is the use of the CI method which has limited performance in examining neuromuscular changes. There are a lot of advanced methods that can be tried and may lead to improved outcome.

More advanced methods including sophisticated spatial filtering methods and more sufficient diagnostic indicators can be used for improved performance. All these efforts remain our future work.

5. Conclusion

This paper examined the feasibility of performing spatial filtering methods using the PCA algorithm, the NMF algorithm and their combination, for enhancing HD-sEMG examination of neuromuscular changes. The experimental results demonstrated that spatial filtering of HD-sEMG can help to improve diagnostic power of CI method with respect to that with no spatial filtering, and that the combined PCA-NMF-based spatial filtering method yielded the highest diagnostic power in identifying complex neuromuscular diseases following SCI. The proposed method facilitate HD-sEMG examination of neuromuscular changes and it helps to develop a standard pipeline for pre-processing the HD-sEMG data towards practical and meaningful applications.

Abbreviations

HD: high-density; sEMG: surface electromyogram; PCA: principle component analysis; NMF: non-negative matrix factorization; CI: clustering index; SCI: spinal cord injury; MU: motor unit; APB: abductor pollicis brevis; MVC: maximal voluntary contraction; PC: principal component (PC); ADI: abnormality discriminating index.

Acknowledgements

The authors would like to acknowledge the participation of all subjects in this study.

Funding

This work was supported in part by the National Natural Science Foundation of China under Grant No. 61771444.

Availability of data and materials

The datasets of the experiments in the current study are available from the first author on request.

Author's contributions

XZ, XL, XT and XuC designed this study. All authors conceived the experiments. XZ and PZ conducted the experiments. XZ, XL, XT, XuC and XiC performed data analyses and interpretations. XZ and XL drafted the manuscript. XuC and PZ substantially revised the manuscript. All authors read and approved the final version of the manuscript.

Ethics approval

The study was approved by the Institutional Review Board of the Northwestern University (Chicago, IL). All subjects signed informed and written consent before any procedure of the experiments.

Consent for publication

The authors consent this article for publication of Journal of NeuroEnginnering and Rehabilitation

Competing interests

The authors declare that they have no competing interests.

References:

[1] Marino R J, Barros T, Biering-Sorensen F, et al. International standards for neurological classification of spinal cord injury[J]. The journal of spinal cord medicine, 2003, 26(sup1): S50-S56.

[2] Zijdewind I, Thomas C K. Motor unit firing during and after voluntary contractions of human thenar muscles weakened by spinal cord injury[J]. Journal of neurophysiology, 2003, 89(4): 2065-2071.

[3] Yang J F, Stein R B, Jhamandas J, et al. Motor unit numbers and contractile properties after spinal cord injury[J]. Annals of Neurology: Official Journal of the American Neurological Association and the Child Neurology Society, 1990, 28(4): 496-502.

[4] Sonoo M. New attempts to quantify concentric needle electromyography[J]. Muscle & Nerve: Official Journal of the American Association of Electrodiagnostic Medicine, 2002, 25(S11): S98-S102.

[5] Hogrel J Y. Clinical applications of surface electromyography in neuromuscular

disorders[J]. Neurophysiologie Clinique/Clinical Neurophysiology, 2005, 35(2-3): 59-71.

[6] Farina D, Cescon C, Merletti R. Influence of anatomical, physical, and detection-system parameters on surface EMG[J]. Biological cybernetics, 2002, 86(6): 445-456.

[7] Lowery M M, Stoykov N S, Taflove A, et al. A multiple-layer finite-element model of the surface EMG signal[J]. IEEE Transactions on Biomedical Engineering, 2002, 49(5): 446-454.

[8] Beck R B J, Houtman C J, O'Malley M J, et al. A technique to track individual motor unit action potentials in surface EMG by monitoring their conduction velocities and amplitudes[J]. IEEE transactions on biomedical engineering, 2005, 52(4): 622-629.

[9] Hogrel J Y. Clinical applications of surface electromyography in neuromuscular disorders[J]. Neurophysiologie Clinique/Clinical Neurophysiology, 2005, 35(2-3): 59-71.

[10] Hogrel J Y. Clinical applications of surface electromyography in neuromuscular disorders[J]. Neurophysiologie Clinique/Clinical Neurophysiology, 2005, 35(2-3): 59-71.

[11] Meekins G D, So Y, Quan D. American Association of Neuromuscular & Electrodiagnostic Medicine evidenced‐based review: Use of surface electromyography in the diagnosis and study of neuromuscular disorders[J]. Muscle & Nerve: Official Journal of the American Association of

669 Electrodiagnostic Medicine, 2008, 38(4): 1219-1224.
670 [12] Kaplanis P A, Pattichis C S, Zazula D. Multiscale entropy-based approach to
671 automated surface EMG classification of neuromuscular disorders[J]. Medical
672 & biological engineering & computing, 2010, 48(8): 773-781.
673 [13] Ferrari D, Kuriki H U, Silva C R, et al. Diagnostic accuracy of the
674 electromyography parameters associated with anterior knee pain in the
675 diagnosis of patellofemoral pain syndrome[J]. Archives of physical medicine
676 and rehabilitation, 2014, 95(8): 1521-1526.
677 [14] Jensen R, Fuglsang-Frederiksen A, Olesen J. Quantitative surface EMG of
678 pericranial muscles in headache. A population study[J]. Clinical
679 Neurophysiology, 1994, 93(5): 335-344.
680 [15] Kaplanis P A, Pattichis C S, Zazula D. Multiscale entropy-based approach to
681 automated surface EMG classification of neuromuscular disorders[J]. Medical
682 & biological engineering & computing, 2010, 48(8): 773-781.
683 [16] Uesugi H, Sonoo M, Stålberg E, et al. “Clustering Index method”: A new
684 technique for differentiation between neurogenic and myopathic changes using
685 surface EMG[J]. Clinical Neurophysiology, 2011, 122(5): 1032-1041.
686 [17] Zhang X, Wei Z, Ren X, et al. Complex neuromuscular changes post-stroke
687 revealed by clustering index analysis of surface electromyogram[J]. IEEE
688 Transactions on Neural Systems and Rehabilitation Engineering, 2017, 25(11):
689 2105-2112.
690 [18] Uesugi H, Sonoo M, Stalberg E, et al. A new technique of analysing surface

691 EMG on voluntary contraction which can differentiate between neurogenic and
692 myopathic changes: a proporsal of clustering index[J]. Clin Neurophysiol, 2000,
693 111(13): 2343-4.
694 [19] Higashihara M, Sonoo M, Yamamoto T, et al. Evaluation of spinal and bulbar
695 muscular atrophy by the clustering index method[J]. Muscle & nerve, 2011,
696 44(4): 539-546.
697 [20] Zhang X, Zhou P. Clustering index analysis of the surface electromyogram
698 poststroke[C]//2013 6th International IEEE/EMBS Conference on Neural
699 Engineering (NER). IEEE, 2013: 1586-1589.
700 [21] Uesugi H, Sonoo M, Stålberg E, et al. “Clustering Index method”: A new
701 technique for differentiation between neurogenic and myopathic changes using
702 surface EMG[J]. Clinical Neurophysiology, 2011, 122(5): 1032-1041.
703 [22] Al Harrach M, Boudaoud S, Gamet D, et al. Evaluation of HD-sEMG
704 probability density function deformations in ramp exercise[C]//2014 36th
705 Annual International Conference of the IEEE Engineering in Medicine and
706 Biology Society. IEEE, 2014: 2209-2212.
707 [23] Huang C, Chen X, Cao S, et al. Muscle-tendon units localization and activation
708 level analysis based on high-density surface EMG array and NMF algorithm[J].
709 Journal of neural engineering, 2016, 13(6): 066001. Medical & biological
710 engineering & computing, 2018, 56(3): 341-353.
711 [24] Liu Y, Ning Y, Li S, et al. Three-dimensional innervation zone imaging from
712 multi-channel surface EMG recordings[J]. International journal of neural

systems, 2015, 25(06): 1550024.

[25] Drost G E A, Stegeman D F, Schillings M L, et al. Motor unit characteristics in healthy subjects and those with postpoliomyelitis syndrome: A high‐density surface EMG study[J]. Muscle & Nerve: Official Journal of the American Association of Electrodiagnostic Medicine, 2004, 30(3): 269-276.

[26] Zhang C, Chen X, Cao S, et al. HD-sEMG-based research on activation heterogeneity of skeletal muscles and the joint force estimation during elbow flexion[J]. Journal of neural engineering, 2018, 15(5): 056027.

[27] Maathuis E M, Drenthen J, van Dijk J P, et al. Motor unit tracking with high-density surface EMG[J]. Journal of Electromyography and Kinesiology, 2008, 18(6): 920-930.

[28] Staudenmann D, Kingma I, Daffertshofer A, et al. Improving EMG-based muscle force estimation by using a high-density EMG grid and principal component analysis[J]. IEEE Transactions on Biomedical Engineering, 2006, 53(4): 712-719.

[29] Al Harrach M, Afsharipour B, Boudaoud S, et al. Extraction of the Brachialis muscle activity using HD-sEMG technique and Canonical Correlation Analysis[C]//2016 38th Annual International Conference of the IEEE Engineering in Medicine and Biology Society (EMBC). IEEE, 2016: 2378-2381.

[30] Chen X, Wang S, Huang C, et al. ICA-based muscle–tendon units localization and activation analysis during dynamic motion tasks[J]. Medical & biological

735 engineering & computing, 2018, 56(3): 341-353.
736 [31] Gazzoni M, Celadon N, Mastrapasqua D, et al. Quantifying forearm muscle
737 activity during wrist and finger movements by means of multi-channel
738 electromyography[J]. PloS one, 2014, 9(10): e109943.
739 [32] Naik G R, Nguyen H T. Nonnegative matrix factorization for the identification
740 of EMG finger movements: Evaluation using matrix analysis[J]. IEEE journal
741 of biomedical and health informatics, 2014, 19(2): 478-485.
742 [33] Golub G H, Van Loan C F. Matrix computations[M]. JHU press, 2012.
743 [34] Daffertshofer A, Lamoth C J C, Meijer O G, et al. PCA in studying coordination
744 and variability: a tutorial[J]. Clinical biomechanics, 2004, 19(4): 415-428.
745 [35] Brown J D. Statistics Corner Questions and answers about language testing
746 statistics: Principal components analysis and exploratory factor
747 analysis—Definitions, differences, and choices[J]. 2009.
748 [36] Valle S, Li W, Qin S J. Selection of the number of principal components: the
749 variance of the reconstruction error criterion with a comparison to other
750 methods[J]. Industrial & Engineering Chemistry Research, 1999, 38(11):
751 4389-4401.
752 [37] Staudenmann D, Kingma I, Daffertshofer A, et al. Heterogeneity of muscle
753 activation in relation to force direction: a multi-channel surface
754 electromyography study on the triceps surae muscle[J]. Journal of
755 Electromyography and Kinesiology, 2009, 19(5): 882-895.
756 [38] Huang C, Chen X, Cao S, et al. An isometric muscle force estimation

framework based on a high-density surface EMG array and an NMF algorithm[J]. Journal of neural engineering, 2017, 14(4): 046005.

[39] Zhou P, Li X, Jahanmiri-Nezhad F, et al. Duration of observation required in detecting fasciculation potentials in amyotrophic lateral sclerosis using high-density surface EMG[J]. Journal of neuroengineering and rehabilitation, 2012, 9(1): 78.

[40] Buciu I. Non-negative matrix factorization, a new tool for feature extraction: theory and applications[J]. International Journal of Computers, Communications and Control, 2008, 3(3): 67-74.

[41] Rafuse V F, Gordon T. Self-reinnervated cat medial gastrocnemius muscles. II. Analysis of the mechanisms and significance of fiber type grouping in reinnervated muscles[J]. Journal of neurophysiology, 1996, 75(1): 282-297.

[42] Thomas C K, Bakels R, Klein C S, et al. Human spinal cord injury: motor unit properties and behaviour[J]. Acta physiologica, 2014, 210(1): 5-19.

[43] Gabriel D A, Kamen G. Experimental and modeling investigation of spectral compression of biceps brachii SEMG activity with increasing force levels[J]. Journal of Electromyography and Kinesiology, 2009, 19(3): 437-448.

[44] Tresch, M.C.; Cheung, V.C.; d'Avella, A. Matrix factorization algorithms for the identification of muscle synergies: Evaluation on simulated and experimental data sets. J. Neurophysiol. 2006, 95, 2199–2212.

[45] Thomas C K, Zaidner E Y, Calancie B, et al. Muscle weakness, paralysis, and atrophy after human cervical spinal cord injury[J]. Experimental neurology,

1997, 148(2): 414-423.

[46] Grumbles R M, Thomas C K. Motoneuron death after human spinal cord injury [J]. Journal of neurotrauma, 2017, 34(3): 581-590.

783 Table 1. Physical characteristic of subjects with spinal cord injury

ID #	Gender	Age (years)	Level of Injury	ASIA Class	Years Since Injury
S1	F	37	C7	C	4
S2	M	57	C7	D	17
S3	M	32	C6	C	11
S4	F	42	C4	D	7
S5	M	62	C4	D	8
S6	M	44	C5	C	11
S7	M	54	C4	D	12
S8	M	38	C7	C	12
S9	F	50	C8	D	7

784

785

786 Table 2. The ADI values derived from different methods

Condition	Left	Right
CH28	6.2292	3.4041
CH31	14.0252	5.7445
CH37	7.7690	2.5341
CH64	2.3160	2.7312
Simply Averaging	2.4936	2.1671
PCA-based	3.1488	3.8785
NMF-based	8.0397	3.8033
PCA-NMF-based	13.9157	11.7014

787

Figure Captains

Fig 1 The flexible electrode array of 64 monopolar electrodes arranged in an 8×8 grid formation.

Fig 2 Block diagram of the framework for examining neuromuscular changes using the CI method and the spatial filtering analyses.

Fig 3 The CI-area plot of a deliberately channel presented in double logarithmic scale for the three groups: SCI-left group, SCI-right group and control group. The normal range (dotted line) is presented within +2.5 of the standard error of the linear regression. The red dots and black circles represent the epochs of SCI-left group and SCI-right group were found to be outside the banding region.

Fig 4 Z-scores derived from four selected channels: (a) channel 28, (b) channel 31, (c) channel 37 and (d) channel 64. The Z-scores from SCI-left group, SCI-right group and control group are shown separately. The normal range (solid line) is presented within ±2.5

Fig 5 Z-scores derived from four methods: (a) simply averaging, (b) PCA spatial filtering, (c) NMF spatial filtering, and (d) PCA-NMF-based spatial filtering. The Z-scores from SCI-left group, SCI-right group and control group are shown separately. The normal range (solid line) is presented within ±2.5.

Figures

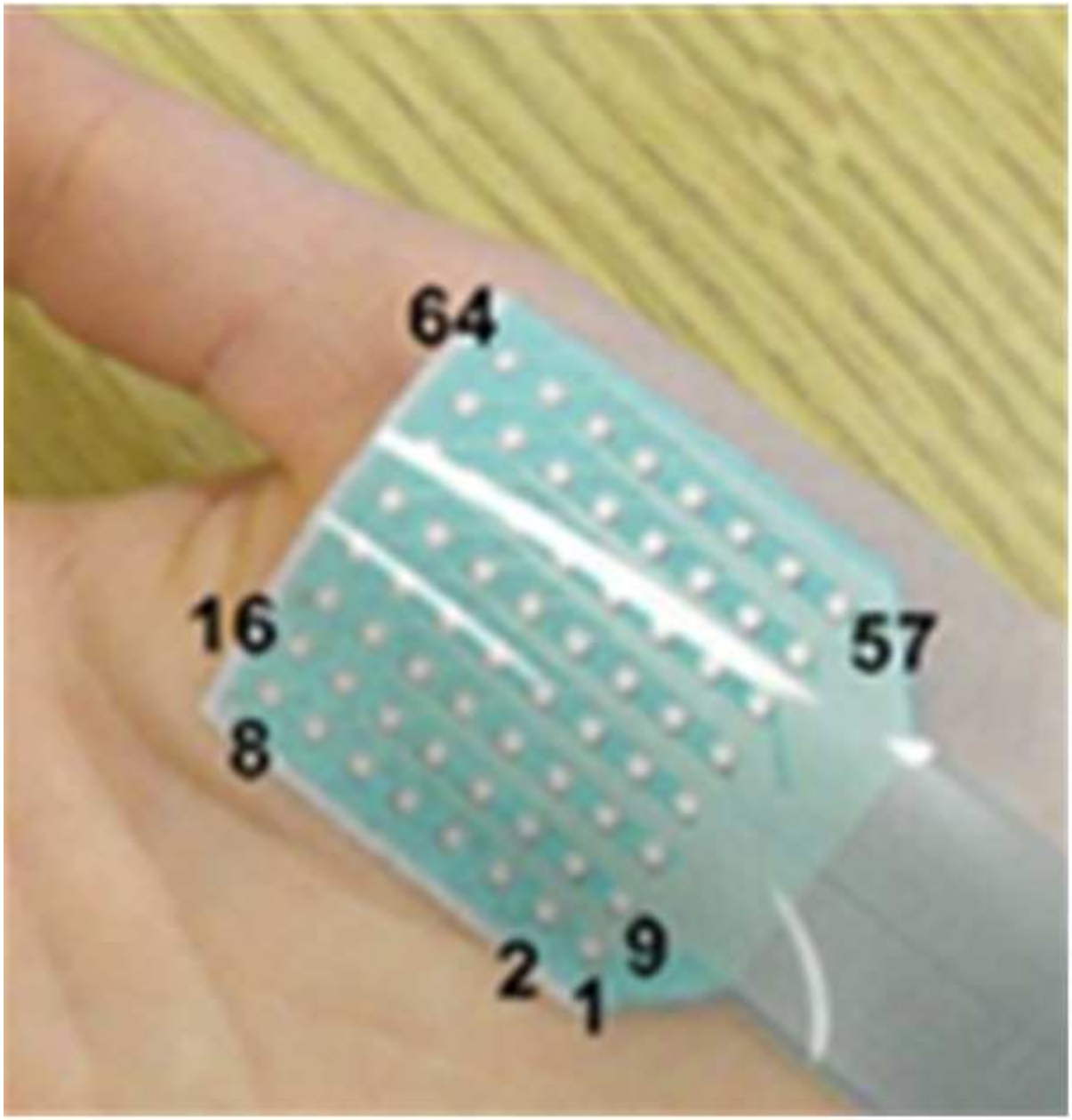

Figure 1

The flexible electrode array of 64 monopolar electrodes arranged in an 8×8 grid formation.

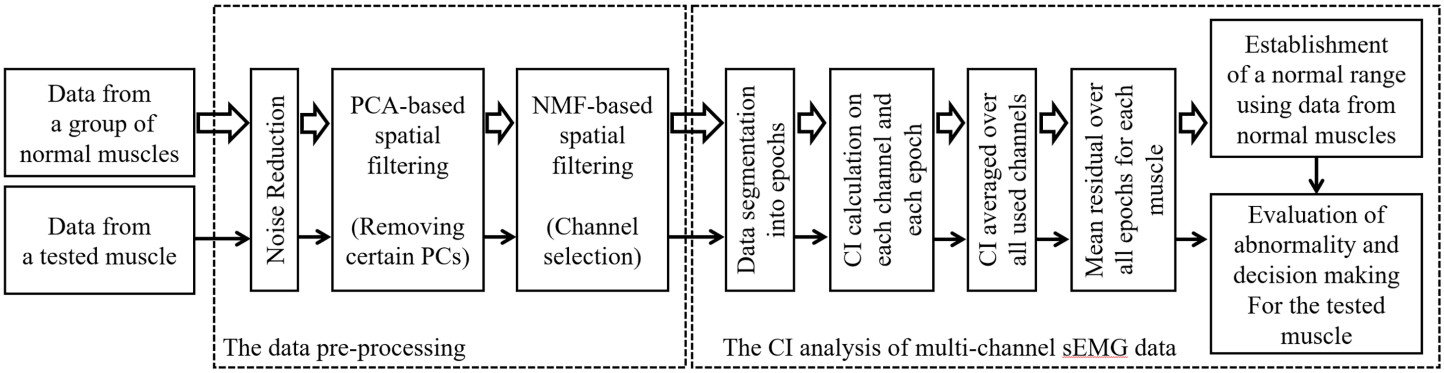

Figure 2

Block diagram of the framework for examining neuromuscular changes using the CI method and the spatial filtering analyses.

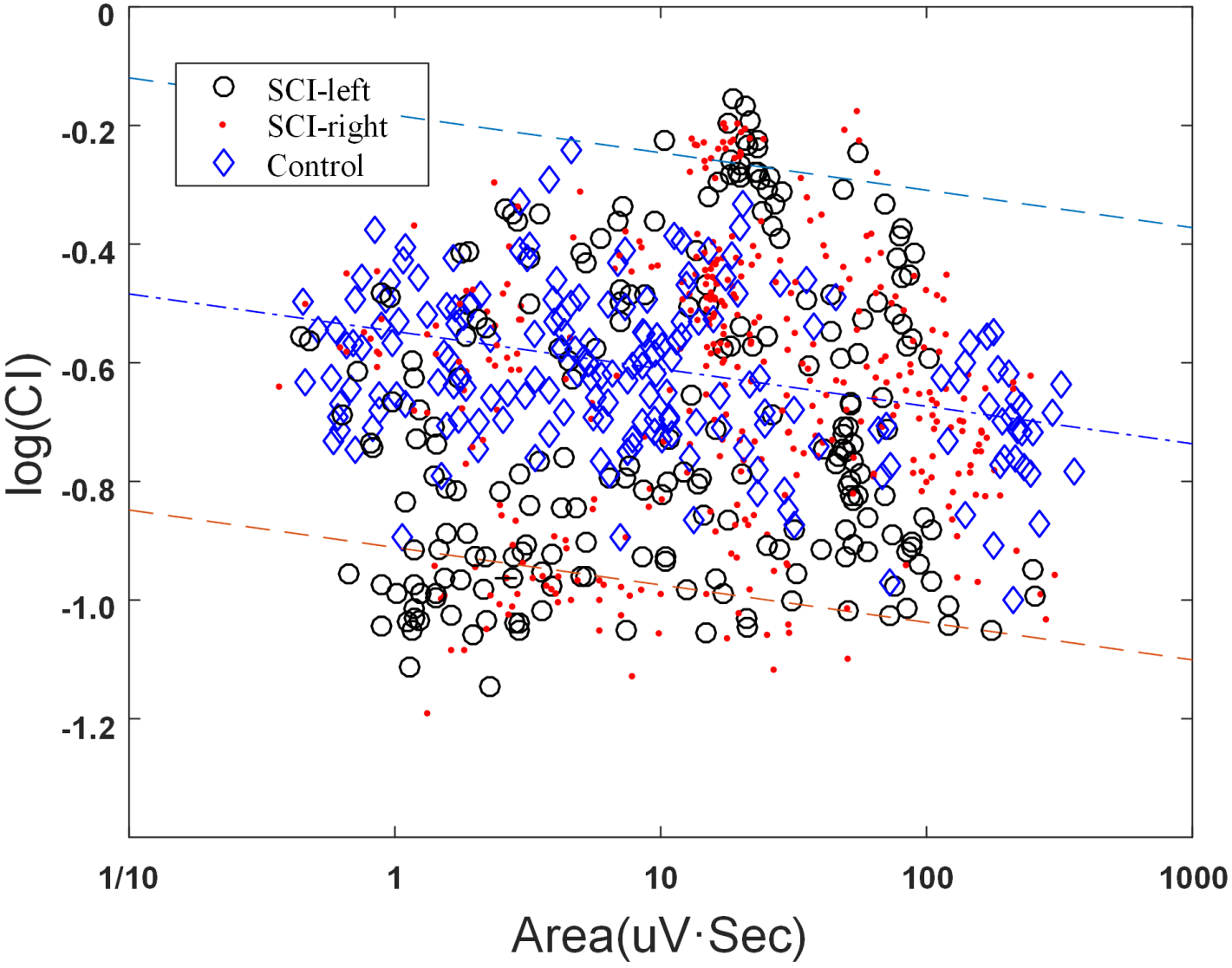

Figure 3

The CI-area plot of a deliberately channel presented in double logarithmic scale for the three groups: SCI-left group, SCI-right group and control group. The normal range (dotted line) is presented within +2.5 of the standard error of the linear regression. The red dots and black circles represent the epochs of SCI-left group and SCI-right group were found to be outside the banding region.

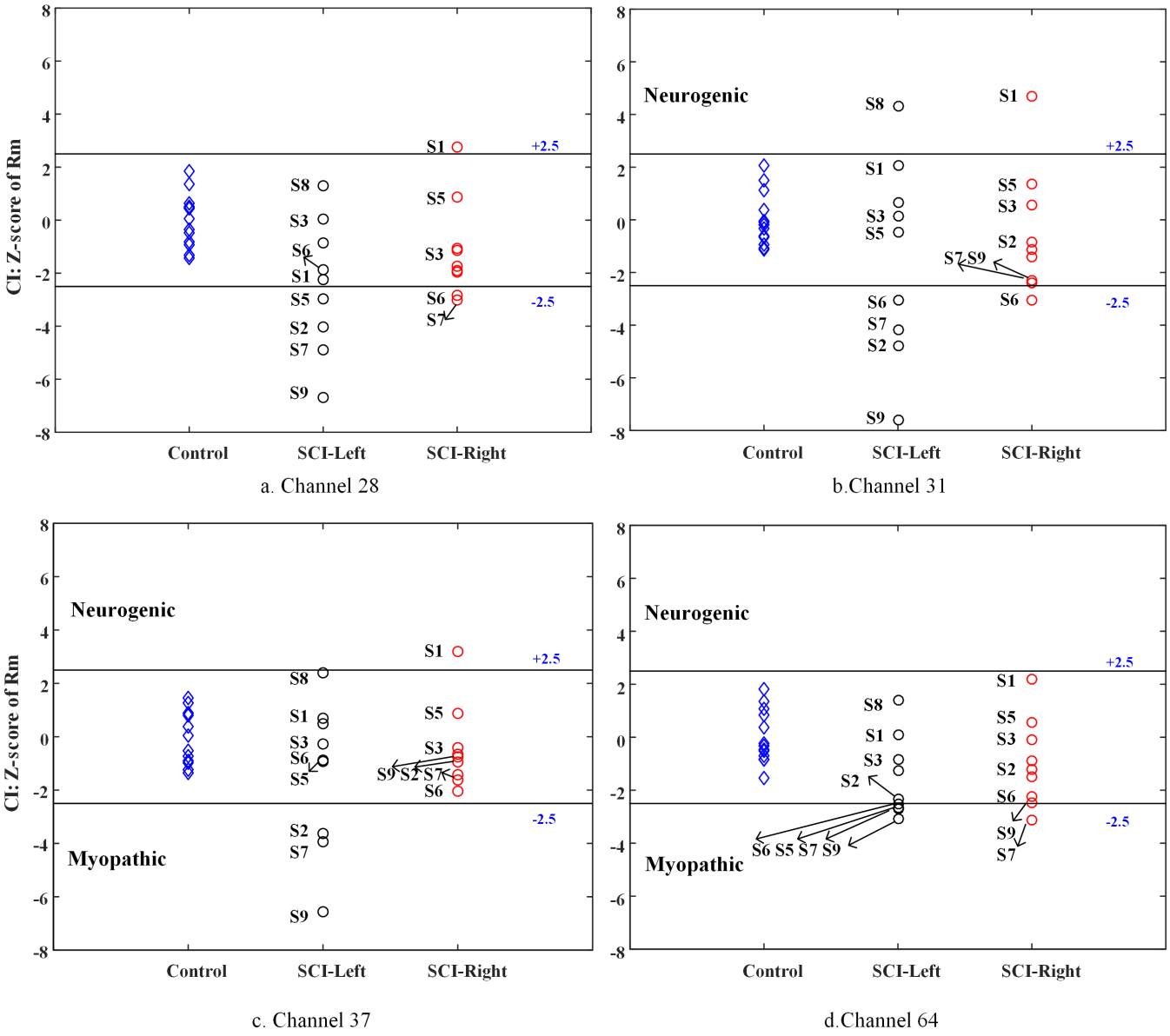

Figure 4

Z-scores derived from four selected channels: (a) channel 28, (b) channel 31, (c) channel 37 and (d) channel 64. The Z-scores from SCI-left group, SCI-right group and control group are shown separately. The normal range (solid line) is presented within ±2.5

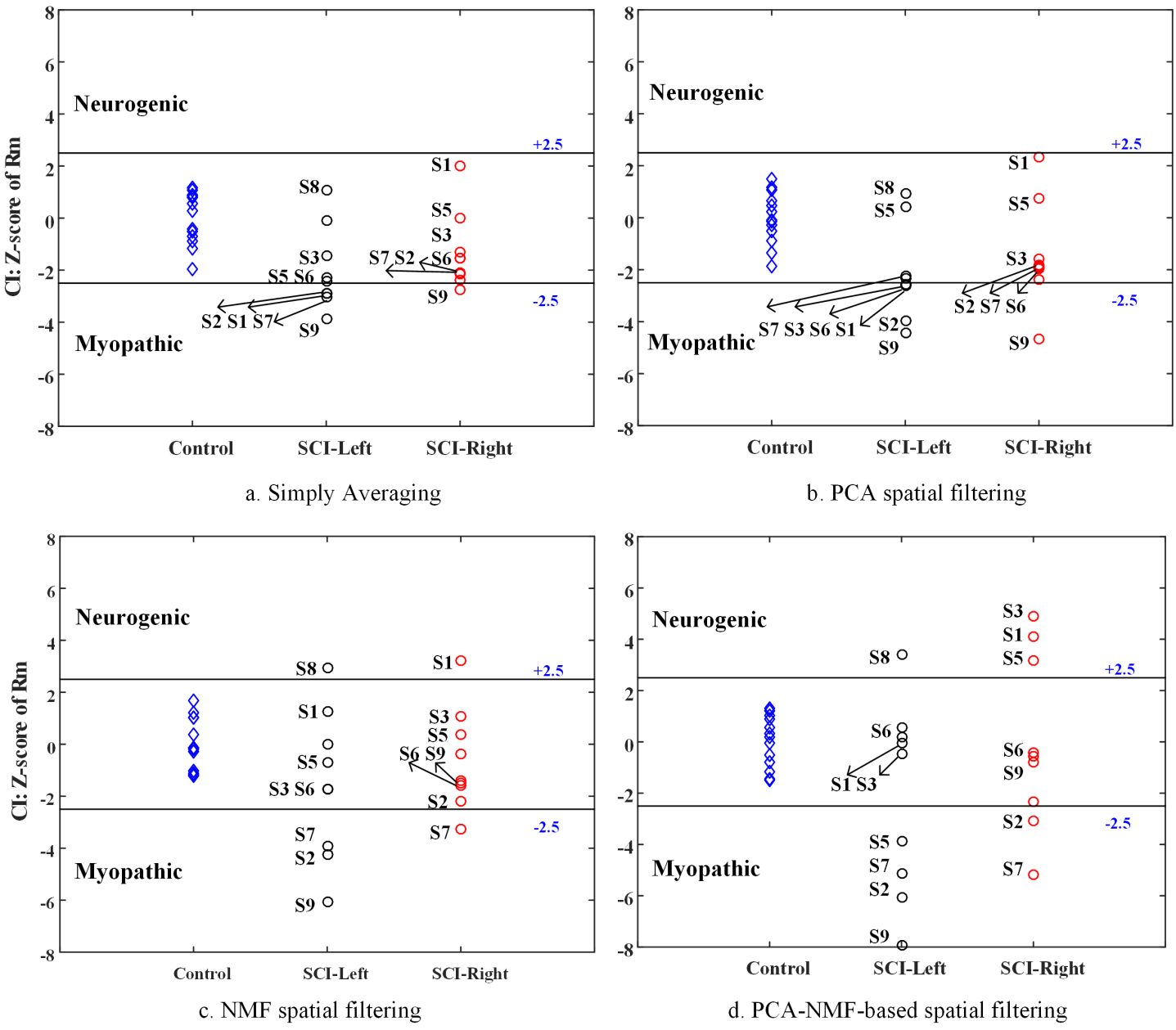

Figure 5

Z-scores derived from four methods: (a) simply averaging, (b) PCA spatial filtering, (c) NMF spatial filtering, and (d) PCA-NMF-based spatial filtering. The Z-scores from SCI-left group, SCI-right group and control group are shown separately. The normal range (solid line) is presented within ±2.5.